1-1-2014

3D FEM analysis of strip shape during multi-pass rolling in a 6-high CVC cold rolling mill

Kezhi Linghu
Shougang Research Institute of Technology, kezhi@uow.edu.au

Zhengyi Jiang
University of Wollongong, jiang@uow.edu.au

Jingwei Zhao
University of Wollongong, jzhao@uow.edu.au

Fei Li
Shougant Research Institute of Technology

Dongbin Wei
University of Wollongong, dwei@uow.edu.au

See next page for additional authors

Recommended Citation

Linghu, Kezhi; Jiang, Zhengyi; Zhao, Jingwei; Li, Fei; Wei, Dongbin; Xu, Jianzhong; Zhang, Xiaoming; and Zhao, Xianming, "3D FEM analysis of strip shape during multi-pass rolling in a 6-high CVC cold rolling mill" (2014). *Faculty of Engineering and Information Sciences - Papers: Part A*. 2743.
https://ro.uow.edu.au/eispapers/2743

3D FEM analysis of strip shape during multi-pass rolling in a 6-high CVC cold rolling mill

Abstract

A 3D elastic–plastic finite element method (FEM) model of cold strip rolling for 6-high continuous variable crown (CVC) control rolling mill was developed. This model considers the boundary conditions such as accurate CVC curves, total rolling forces, total bending forces and roll shifting values. The rolling force distributions were obtained by the internal iteration processes instead of being treated as model boundary conditions. The calculated error has been significantly reduced by the developed model. Based on the rolling schedule data from a 1,850-mm CVC cold rolling mill, the absolute error between the simulated results and the actual values is obtained to be less than 10 μm and relative error is less than 1 percent. The simulated results are in good agreement with the measured data. The developed model is significant in investigating the flatness control capability of the 6-high CVC cold rolling mill in terms of work roll bending forces, intermediate roll bending forces and intermediate roll shifting values.

Keywords

strip, shape, during, multi, pass, analysis, rolling, fem, 6, high, cvc, cold, mill, 3d

Disciplines

Engineering | Science and Technology Studies

Publication Details

Linghu, K., Jiang, Z., Zhao, J., Li, F., Wei, D., Xu, J., Zhang, X. & Zhao, X. (2014). 3D FEM analysis of strip shape during multi-pass rolling in a 6-high CVC cold rolling mill. The International Journal of Advanced Manufacturing Technology, Online first 1-13.

Authors

Kezhi Linghu, Zhengyi Jiang, Jingwei Zhao, Fei Li, Dongbin Wei, Jianzhong Xu, Xiaoming Zhang, and Xianming Zhao

3D FEM analysis of strip shape during multi-pass rolling in a 6-high CVC cold rolling mill

Kezhi Linghu[1], Zhengyi Jiang[2,*], Jingwei Zhao[2], Fei Li[1], Dongbin Wei[2], Jianzhong Xu[3], Xiaoming Zhang[3], Xianming Zhao[3]

[1]Shougang Research Institute of Technology, Shougang Group, No. 69 Yangzhuang Street, Shijingshan District, Beijing 100043, China.

[2]School of Mechanical, Materials & Mechatronic Engineering, University of Wollongong, Wollongong, NSW 2522, Australia

[3]State Key Laboratory of Rolling and Automation, Northeastern University, Shenyang 110819, China

Abstract:

A 3D elastic-plastic finite element method (FEM) model of cold strip rolling for 6-high continuous variable crown (CVC) control rolling mill was developed. This model considers the boundary conditions such as accurate CVC curves, total rolling forces, total bending forces and roll shifting values. The rolling force distributions were obtained by the internal iteration processes instead of being treated as model boundary conditions. The calculated error has been significantly reduced by the developed model. Based on the rolling schedule data from a 1850 mm CVC cold rolling mill, the absolute error between the simulated results and the actual values is obtained to be less than 10μm, and relative error is less than 1%. The simulated results are in good agreement with the measured data. The developed model is significant in investigating the flatness control capability of the 6-high CVC cold rolling mill in terms of work roll bending, intermediate roll bending and intermediate roll shifting.

Keywords: continuous variable crown; 6-high rolling mill; cold rolling; finite element; flatness

* Corresponding author. Tel: +61-2-42214545; Fax: +61-2-42215474

E-mail addresses:

bjlhkz@139.com (K. Linghu), jiang@uow.edu.au (Z. Jiang), jwzhaocn@gmail.com (J. Zhao).

Nomenclature

α_{i}	coefficients of CVC curve, i is integer index (i=0-4)	FEM	finite element method
α_{ii}	freedom degree, i is integer index (i=1-3)	IMR	intermediate roll
β	non-uniform coefficient	I_{n}	bending force of IMR, n is integer index (n=1-3)
$\gamma_{\mathrm{xy}}, \gamma_{\mathrm{yz}}, \gamma_{\mathrm{zx}}$	shear strains	L_{e}	length of the minimum feature unit
Δt	step time	$[K]$	stiffness matrix
Δt_{cr}	critical step time	$[M]$	mass matrix
ε_{Σ}	accumulated deformation ratio	m_a^e	mass of node α in element e
$\varepsilon_{\mathrm{x}}, \varepsilon_{\mathrm{y}}, \varepsilon_{\mathrm{z}}$	normal strains	M_e	total mass of element e
η	constant less than 1.0	M_{ij}	element of mass matrix $[M]$, i is the row coordinate of $[M]$, j is the column coordinate of $[M]$, $M_{\mathrm{ij}} = 0\ (i \neq j)$, and $M_{\mathrm{ii}} > 0$
μ	Poisson's ratio of the material		
ρ	density of material		
ρ_{α}	density of the node α	$[N]$	shape function matrix
σ_{s}	uniaxial tensile yield strength	N_{e}	number of nodes
$\sigma_{\mathrm{x}}, \sigma_{\mathrm{y}}, \sigma_{\mathrm{z}}$	normal face stresses	$p_{\max}$	maximum value of distribution
$\tau_{\mathrm{xy}}, \tau_{\mathrm{yz}}, \tau_{\mathrm{zx}}$	shear stresses	p_{ave}	average value of distribution
ω	natural frequency of the system	S_{n}	shifting value of IMR, n is integer index (n=1-3)
a_1, a_2, a_3	constants of the model of deformation resistance of strip	T	transpose of matrix
		V	volume of node
BR	back up roll	V^e	volume of the element e
$[C]$	matrix of damping	WR	work roll
C_{r}	strip crown	W_{n}	bending force of WR, n is integer index (n=1-3)
CVC	continuous variable crown	x	coordinate of roll barrel
E	elastic modulus	y	radius of the roll barrel regarding the coordinate of x
E_{d}	strip edge drop		

1. Introduction

Cold rolled strips are widely used in various aspects of national economy such as electric works, automobile, home appliance and light industry. Besides the increasing requirement for quantity of cold rolled strips, customers have been paying more and more attention to the strip shape quality of the rolled products [1]. The strip shape quality mainly consists of flatness control and cross-section control. In order to produce high quality strip, flatness and cross-section control has been extensively employed in cold rolling [2, 3].

How to precisely calculate the internal pressure distribution and elastic-plastic deformation for rolls and strips is a precondition for both the improvement of rolling technology such as optimisation of roll contours and the assessment of flatness control ability of the mill [4, 5]. In the past several decades, different numerical calculations including the elastic base beam method introduced by Stone [6] and the influence function method proposed by Shohet [7] have been applied to study the deformation of the roll set. One of the limitations of these numerical methods, however, is that they can generally only solve the two-dimensional problem [8-10]. The finite element method (FEM) is an effective method for solving various mathematical problems. The principal idea of FEM is to divide the domain into a finite number of non-overlapping units, in which the appropriate node is selected as solving function interpolation point. The variables in the differential equations are rewritten as linear expression that consists of selected interpolation functions and variables or node values of the derivative, and finally the equations can be discretised and solved effectively. FEM has been successfully applied to lots of metal manufacturing industrial processing fields. Precise calculation results can be obtained because of the effectiveness of applying realistic boundary conditions and constrains to the FEM models in complicated cases [11, 12]. Even though FEM modelling of rolling and deformation has made great achievement, the work on the modelling of the strip, rolls and force distribution has just been conducted separately, and the model is usually developed based on the hypotheses of rolling force distribution such as

2-order curve which will definitely reduce the reliability of the calculated results [13, 14]. Particularly in the case of 6-high continuous variables crown (CVC), the introduction of CVC curves of intermediate roll (IMR) makes the rolling force distribution between rolls as well as between the work roll (WR) and the strip more complicated, and the conventional modelling is hard to meet the accuracy requirements. With the rapid development of high performance computer and parallel computing technology [15], it is possible to develop a FEM model to simulate the cold rolling process [16].

In this paper, an accurate 3D FEM model for 6-high CVC rolling mill was developed to analyse the elastic-plastic deformation of strip-roll-coupled overall mill. The complicated rolling force distributions between the rolls as well as between the roll and the strip were accurately solved by the internal iteration of the developed model, which were different with conventional treatment methods [13, 14]. The performance of the developed 3D FEM model has been verified by a comparison between the simulated results and measured data obtained from a 1850 mm CVC cold rolling mill. The developed model was utilised to explore the flatness control ability of the CVC cold rolling mill with respect to the actuators such as WR bending force, IMR bending force and IMR shifting value.

2. 6-high CVC cold rolling mill

2.1. Curve equation of CVC rolls

More than 150 production lines have applied CVC technology around the world since it was developed in 1982 [17]. 6-high CVC cold roll mill is a new generation of high precision strip rolling technology that was developed and successfully applied in practice by Schloemann-Siemag (SMS), Germany [18]. The IMRs of the 6-high CVC cold rolling mill are applied with special contour such as 3rd order [19] and 5th order (CVC plus) curves [20]. The 5th order curve function (function of radius) is expressed as follows [20]:

$$y\ (x) = \alpha_0 + \alpha_1 x + \alpha_2 x^2 + \alpha_3 x^3 + \alpha_4 x^5 \tag{1}$$

where x is the coordinate of roll barrel, y is the radius of the roll barrel regarding the coordinate of x, and α_0, α_1, α_2, α_3, α_4 are coefficients of curves.

With the applications of WR bending, IMR bending, CVC curve and transverse shifting of IMRs, 6-high CVC cold rolling mill features both the powerful flatness control ability and complicated structures compared to the conventional 4-high rolling mill. The rolling force distribution between the rolls and the elastic-plastic deformation of the strip and the roll, which are key factors for the optimisation of rolling technology and flatness improvement in strip rolling, are complicated because of the structure featured by 6-high CVC rolling mill.

2.2. Parameters and contour of rolls

The research in this paper is based on a 1850 mm 6-high CVC rolling mill, as shown in Fig. 1. The arrows in Fig. 1 indicate the definition of the positive directions for WR bending force, IMR bending force and IMR shifting respectively. The WR, IMR and backup roll (BR) are machined with parabolic curve, CVC plus curve and CVC curve, respectively. The parameters of the roll set are shown in Table 1.

The curves of WR, IMR and BR are shown in Fig. 2. It can be seen from Fig. 2a that the curve of WR is symmetrical. This profile feature can, on one hand, compensate the elastic deflection of the WR due to high rolling force and reduce the inhomogeneous deformation along the strip width, on the other hand, it helps to keep rolling stability and make the strip be rolled symmetrically. When the profile of the IMR is machined as a CVC curve (Fig. 2b), it is possible to effectively change the contact conditions between the BR and the WR simultaneously, and then to change the rolling force distribution between rolls. Finally the roll gap can be modified and the delivery flatness of the strip can be controlled. The BR is applied with CVC curve (Fig. 2c) that can match with the curve used by IMR to reduce the uneven wear of rolls.

3. Development of 3D FEM model

The elastic-plastic FEM was developed by Marcal and Yamada [21] in the late 1960s based on the elastic-plastic matrix. With the fast development of FEM and high performance of computer, the FEM modelling of rolling has been changed from single simulation of the contact between the roll and the strip to complicated studying on the contact friction based on elastic-plastic FEM [22-24].

3.1. Elastic-plastic FEM model

Because strip rolling itself is a dynamic process, explicit dynamic elastic-plastic FEM, which is calculated by time difference scheme, is applied to model the cold rolling of strip on the 6-high CVC rolling mill.

3.1.1. Matrix of mass

To simplify the model, the mass matrix derives from the hypothesis that the mass of single element concentrates at the node and the acceleration of the node does not affect the initial force of others nodes [25]. Because the mass matrix of a single FEM element is diagonal, i.e. the non-diagonal element of the matrix is 0, the overall mass matrix $[M]$ is also diagonal, which can be expressed as follows:

$$[M]=\{M_{\mathrm{ij}}\}=\begin{bmatrix} M_{11} & & \cdots & & \cdots & M_{1\mathrm{N}} \\ & M_{22} & & & & \\ \vdots & & \ddots & & & \\ & & & \ddots & M_{ij} & \\ \vdots & & & M_{ji} & \ddots & \\ M_{\mathrm{N}1} & & & & & M_{\mathrm{NN}} \end{bmatrix} \tag{2}$$

where M_{ij} is the element of mass matrix $[M]$, i is the row coordinate of $[M]$, j is the column coordinate of $[M]$, $M_{ij}=0\ (i \neq j)$, and $M_{ii}>0$.

The density of a solid element is assumed to be homogenous, then:

$$m_\alpha^e = \frac{1}{N_e}\int_{V^e}\rho_\alpha dV = \frac{1}{N_e}M_e \tag{3}$$

where m_a^e is the mass of node α in element e, N_e is the number of nodes, ρ_α is the density of the node α, V is the volume of node α, and M_e is the total mass of element e.

3.1.2. Matrix of damping

Assuming the damping force is proportional to the velocity and opposite to the speed direction, the coefficient of damping γ equals to the damping force of unit volume under unit speed. Then the matrix of damping $[C]$ for the model can be expressed as the following form:

$$[C]=\sum\int_{V^e}\gamma[N]^T[N]dV \tag{4}$$

where V^e is the volume of the element, $[N]$ is the shape function matrix of element, T means the transpose of matrix. Because the damping coefficient is relevant to material property and vibration frequency, the damping matrix for the model is determined by the experiment based on mass matrix $[M]$ instead of element damping matrix, the matrix of damping for the model can be rewritten as:

$$[C]=\alpha[M]+\beta[K] \tag{5}$$

where α and β are both constants, and $[K]$ is the stiffness matrix of the model. In general, the cold rolling mill can be treated as a low frequency dynamic system, i.e. $\beta=0$ [26]. Then Eq. (5) becomes:

$$[C]=\alpha[M] \tag{6}$$

where α_{ii} ,the component of α regarding the freedom degree i, can be determined according to the critical vibration condition based on the assumption that the cold rolling mill works in the low frequency:

$$\alpha_{ii} = 2\omega_i \tag{7}$$

where ω_i is the natural frequency of the system.

3.1.3. Step time

In order to run the simulation stably, the step time Δt is set to be less than the critical step time Δt_{cr}. In the case of plastic deformation simulation, Δt can be written in the following form:

$$\Delta t = \eta \Delta t_{cr} \tag{8}$$

where η is a constant less than 1.0. In this paper η is set as 0.7 based on the work of Du [26].

In 3D FEM simulation, the critical step time Δt_{cr} is determined with respect to the FEM element size as follows:

$$\Delta t_{cr} \le L_e \sqrt{\frac{\rho}{E}} \tag{9}$$

where L_e is the length of the minimum feature unit, E is the elastic modulus, and ρ is the density of material.

3.1.4. Relationship between stress and strain

The unit volume stress state is shown in Fig. 3 [25], where the σ_x, σ_y and σ_z are normal face stresses , τ_{xy}, τ_{yz} and τ_{zx} are shear stresses, ε_x, ε_y and ε_z are normal strains, and γ_{xy}, γ_{yz} and γ_{zx} are shear strains which can be written in vector forms as follows:

$$\{\sigma\} = \{\sigma_x, \sigma_y, \sigma_z, \tau_{xy}, \tau_{yz}, \tau_{zx}\}^T \tag{10}$$

$$\{\varepsilon\} = \{\varepsilon_x, \varepsilon_y, \varepsilon_z, \gamma_{xy}, \gamma_{yz}, \gamma_{zx}\}^T \tag{11}$$

The relationship between the stress and strain can be described as: $\{\sigma\} = [D]\{\varepsilon\}$, where $[D]$ is the elasticity matrix of the model that can be described in Eq. (12):

$$
[D]=\frac{E(1-\mu)}{(1+\mu)(1-2\mu)}=\begin{bmatrix} 1 & \frac{\mu}{1-\mu} & \frac{\mu}{1-\mu} & 0 & 0 & 0 \\ \frac{\mu}{1-\mu} & 1 & \frac{\mu}{1-\mu} & 0 & 0 & 0 \\ \frac{\mu}{1-\mu} & \frac{\mu}{1-\mu} & 1 & 0 & 0 & 0 \\ 0 & 0 & 0 & \frac{1-2\mu}{2(1-\mu)} & 0 & 0 \\ 0 & 0 & 0 & 0 & \frac{1-2\mu}{2(1-\mu)} & 0 \\ 0 & 0 & 0 & 0 & 0 & \frac{1-2\mu}{2(1-\mu)} \end{bmatrix} \tag{12}
$$

where E is the elastic modulus, and μ is the Poisson's ratio.

3.2. 3D model of cold rolling mill

To increase the accuracy and reduce the cost of calculation, different meshing strategies were applied to BR, IMR and WR respectively. As shown in Fig. 4, 204167 elements (19214 elements for BR, 21802 elements for IMR, 55334 elements for WR and 107817 elements for strip) and 170468 nodes (5363 nods for BR, 5377 nods for IMR, 13904 nods for WR and 145824 nods for strip) were employed in the model. The modelling of rolls and strip were developed based on elastic and elastic-plastic deformation characteristics, respectively. The hardware configuration of computer is as follows: Intel Core (TM) I7-2600@3.4 GHz for CPU processor, 16GB for RAM, Windows 7 professional 64-bit. It takes about 52 hours to perform a calculation case for the model.

The mechanical properties of rolls for the FEM model are shown in Table 2.

3.3. The model of deformation resistance of strip

3.3.1. Mathematical model

Based on the characteristics of cold rolling that the deformation resistance of low-carbon steel is primarily related to the accumulated deformation, the following mathematic model was selected to describe the relationship between the accumulated deformation and deformation resistance [10, 27].

$$\sigma_s = a_1 \times (\varepsilon_\Sigma + a_2)^{a_3} \tag{13}$$

where σ_s is the uniaxial tensile yield strength of steel, ε_Σ is the accumulated deformation ratio of steel, and a_1, a_2 and a_3 are constants.

3.3.2. Experimental data

24 specimens were taken from the studied steel and were treated with pickling, and then the specimens were rolled with different reductions. σ_s of the rolled specimens was evaluated by room temperature tensile tests, and the values are shown in Table 3. Fig. 5 shows the curve fitting of deformation resistance of the steel.

The fitted coefficients are shown in Table 4. The relationship between the reduction and deformation resistance can be described by Eq. (14).

$$\sigma_s = 124.21327 \times (100 \times \varepsilon_\Sigma + 9.65792)^{0.38578} \tag{14}$$

4. Results analysis and model validation

Table 5 shows a 5-pass rolling schedule from 1850 mm cold rolling mill. The entry thickness of incoming material is 5.4 mm, exit thickness is 1.96 mm, width is 1246 mm and total reduction is 63.7%.

4.1. Rolling force distribution

Due to the application of CVC curves in cold rolling mill, the rolling force distribution between the BR and IMR features the characterisation of ‘S’ shape, and the rolling force distribution between the strip and WR transforms to be symmetrical by the application of crowned WR. The stress contour of the simulated result is shown in Fig. 6. Fig. 7 shows the rolling force distributions between rolls as well as between the roll and the strip for the third pass. It is clear that the rolling force distribution transforms from 'S' shape between the BR and IMR (Fig. 7a) to symmetrical shape between the WR and the strip (Fig. 7c).

4.2. Comparison of thickness distribution

The inter-stand samples were taken from cold rolling mill to compare the difference between the simulated results and actual values. The measured position of the inter-stand specimen is shown in Fig.8.

The comparison between the simulated results and measured data is shown in Fig. 9, in which the solid lines ($\times$) stand for the actual thickness, and the dashed lines ($\circ$) stand for the simulated results. It can be seen that the simulated results agree well with the actual measured values with exception of local bump points caused by the incoming material and their counterpart points in the following stands. The average absolute error across the transection of the strip between the simulated and measured values is less than 10 μm, and average relative error is less than 1%. The developed model validates the excellent capability of simulating the cold strip rolling process.

5. Evaluation of flatness control capability

The flatness control of strip involves essentially the strip cross-sectional contour control, in particularly the crown and edge drop control [28-30]. The definitions of crown and edge drop are shown in Fig. 10. h_{e} is the thickness of the strip at the point B which is e mm away from the left edge (OS). h_{i} and h_{j} have the similar meaning with that of h_{e}. $h_{\mathrm{e'}}$, $h_{\mathrm{i'}}$ and $h_{\mathrm{j'}}$ are the counterparts of the h_{e}, h_{i} and h_{j} at the right side (DS). h_{c} is the thickness of the strip at the central point.

The strip edge drop E_{d} is defined as [1]:

$$E_{\mathrm{d}} = \left[\left(h_{\mathrm{j}} - h_{\mathrm{e}}\right) + \left(h_{\mathrm{j'}} - h_{\mathrm{e'}}\right)\right]/2 \tag{15}$$

The strip crown C_r is defined as [1]:

$$C_r = h_c - (h_i + h_{i'})/2 \tag{16}$$

where $e = e' = 15$ mm, $i = i' = 45$ mm, and $j = j' = 115$ mm.

In order to simplify the model, three symbols (W_n, I_n and S_n) that specify the condition of flatness control are defined in Table 6. The flatness control ability of 6-high CVC cold rolling mill was explored systematically by the developed 3D model in terms of crown and edge drop.

5.1. Characteristics of crown control

5.1.1. Effect of WR bending force

Fig. 11 shows the strip crown change trends with respect to WR bending force. It can be seen that the strip crown changes nonlinearly with WR bending force. In the cases of $I_2\_S_2$ and $I_3\_S_2$, the values of strip crowns increase gradually with WR bending force. For $I_3\_S_3$, however, the strip crown shows a decreasing trend with WR bending force. In the cases of $I_1\_S_3$ and $I_3\_S_1$, strip crown increases and then decreases with an increase of WR bending force. For $I_1\_S_1$, $I_1\_S_2$, $I_2\_S_1$ and $I_2\_S_3$, however, the strip crown decreases and then increases with an increase of WR bending force.

5.1.2. Effect of IMR bending force

Fig. 12 shows strip crown change trends with respect to IMR bending force. It can be seen that the strip crown changes nonlinearly with IMR bending force. In the case of $W_1\_S_1$ the values of strip crowns increase gradually with intermediate bending force. For $W_2\_S_2$ and $W_3\_S_3$, however, the strip crown shows a decreasing trend with IMR bending force. In the cases of $W_1\_S_3$, $W_2\_S_1$ and $W_3\_S_1$, the strip crown increases and then decreases with an increase of IMR bending force. For $W_1\_S_2$, $W_2\_S_3$ and $W_3\_S_2$, however, the strip crown decreases and then increases with an increase of IMR bending force.

5.1.3. Effect of IMR shifting value

Fig. 13 shows the strip crown change trends with respect to IMR shifting value. It can be seen that the strip crown changes nonlinearly with IMR shifting value. In the cases of $W_1\_I_2$, $W_2\_I_2$, $W_3\_I_2$ and $W_3\_I_3$, the values of strip crown shows a decreasing trend with IMR shifting value. In the cases of $W_1\_I_3$, $W_2\_I_1$, $W_2\_I_3$ and $W_3\_I_1$, the strip crown increases and then decreases with an increase of IMR shifting value. For $W_1\_I_1$, however, the strip crown decreases and then increases with an increase of IMR shifting value.

5.2. Characteristics of edge drop control

5.2.1. Effect of WR bending force

Fig. 14 shows the strip edge drop change trends with respect to WR bending force. It can be seen that the strip edge drop changes nonlinearly with WR bending force. In the cases of $I_1\_S_1$, $I_1\_S_2$, $I_2\_S_1$, $I_2\_S_2$, $I_2\_S_3$, $I_3\_S_1$, $I_3\_S_2$ and $I_3\_S_3$, the strip edge drops show a decreasing trend with WR bending force. In the case of $I_1\_S_3$, however, the strip edge drop increases and then decreases with an increase of WR bending force.

5.2.2. Effect of IMR bending force

Fig. 15 shows the strip edge drop change trends with respect to IMR bending force. It can be seen that the strip edge drop changes nonlinearly with IMR bending force. In the cases of $W_1\_S_1$, $W_1\_S_2$, $W_1\_S_3$, $W_2\_S_2$, $W_3\_S_1$, $W_3\_S_2$ and $W_3\_S_3$, the strip edge drops show a decreasing trend with IMR bending force.

In the case of $W_2\_S_1$, strip edge drop increases and then decreases with an increase of IMR bending force. In the case of $W_2\_S_3$, however, the strip edge drop increases and then decreases with an increase of IMR bending force.

5.2.3. Effect of IMR shifting value

Fig. 16 shows strip edge drop change trends with respect to IMR shifting value. It can be seen that the strip edge drop changes nonlinearly with IMR shifting value. In the cases of $W_1\_I_1$, $W_1\_I_2$, $W_2\_I_2$, $W_2\_I_3$, $W_3\_I_1$, $W_3\_I_2$ and $W_3\_I_3$, the strip edge drops show a decreasing trend with IMR shifting value. In the case of $W_2\_I_1$, strip edge drop increases and then decreases with an increase of IMR shifting value. In the case of $W_1\_I_3$, however, strip edge drop increases and then decreases with an increase of IMR shifting value.

5.3. Mechanism of CVC IMR shifting on flatness control

In order to further study the mechanism of shifting values of 6-high CVC cold rolling mill on flatness control, the simulated rolling force distribution between the IMR and WR, the rolling force distribution between the WR and strip, and the transverse thickness distribution of strip were analysed and compared based on the developed 3D model. The distributions of rolling force and profile regarding shifting value of $W_2\_I_2\_S_1$, $W_2\_I_2\_S_2$, $W_2\_I_2\_S_3$ are shown in Fig. 17.

It can be seen from Fig. 17(a) that the rolling force at the both ends of WR are lower than that in the central region. In addition, the rolling force of $W_2\_I_2\_S_2$ is higher than that of both the $W_2\_I_2\_S_1$ and $W_2\_I_2\_S_3$ at the both ends of the strip. In the central region, however, $W_2\_I_2\_S_3$ shows the highest rolling force in contrast to others. Consequently, the total rolling force is kept as a constant. From Fig. 17(b), it can be seen that the rolling force on the both ends of WR are higher than that in the central region. In addition, the force of $W_2\_I_2\_S_2$ is higher than that of both the $W_2\_I_2\_S_1$ and $W_2\_I_2\_S_3$ at the both ends of the strip. In the central region, however, $W_2\_I_2\_S_3$ shows the highest force in contrast to others. Similarly, the total rolling force is kept as a constant. From Fig. 17(c), it can be seen that the thickness distribution of strip on the both ends are lower than that in the central region. In addition, the thickness of $W_2\_I_2\_S_3$ is higher than that of both the $W_2\_I_2\_S_1$ and $W_2\_I_2\_S_2$ at the both ends of the strip. In the central region, however, $W_2\_I_2\_S_2$ shows the highest thickness in contrast to others, and the total area of the strip cross section is kept as a constant. As shown in Fig. 17(d), both the strip crown and the strip edge drop decrease gradually with an increase of IMR shifting value.

To quantitatively analyse the effect of CVC shifting value on flatness control, a non-uniform coefficient β is defined as follows:

$$\beta = \frac{p_{\max}}{p_{\mathrm{ave}}} \tag{17}$$

where $p_{\max}$ is the maximum value of distribution, p_{ave} is the average value of distribution .

Three non-uniform coefficients, β_{iw} (non-uniform coefficient of the rolling force distribution between the IMR and the WR), β_{ws} (non-uniform coefficient of the rolling force distribution between the WR and the strip) and β_{sp} (non-uniform coefficient of the strip profile), regarding different CVC shifting values are shown in Table 7 respectively. It can be seen that as the value of IMR shifting is changed, β_{iw} , β_{ws} and β_{sp} are modified simultaneously. Consequently, both the crown and the edge drop (Fig.17(c)) of the strip are changed. So, the shifting value of the IMR of 6-high CVC cold rolling mill is an effective approach for the strip flatness control.

6. Conclusions

1) A 3D FEM model was developed to characterise the rolling force distributions between rolls as well as between the roll and the strip of a CVC 6-high cold rolling mill. The work hardening effect was considered through room temperature tensile tests after different reductions.

2) The model was validated by a comparison between the simulated results and the measured values. The average absolute error between the simulated results and the actual values was less than 10μm, and the relative error was less than 1%.

3) The flatness control ability of 6-high CVC cold rolling mill was evaluated based on the developed FEM model. The results showed that the WR bending, IMR bending and IMR shifting were effective actuators to control the strip flatness (strip crown and edge drop). Generally, the strip edge drop decreases gradually with the increase of WR bending, IMR bending and IMR shifting values.

4) The developed 3D FEM model for 6-high CVC cold rolling mill shows an excellent ability for simulating the cold strip rolling process, and provides an effective approach for the optimisation of roll contours and improvement of flatness.

References

1. Ginzburg VB (1993) High-quality steel rolling: theory and practice. Marcel Dekker Inc., New York, USA
2. Chen X (1997) Flatness control in new generation high-tech mill for wide strip rolling. J Univ Sci Technol Beijing 19:1-5
3. Ginzburg VB (1993) Profile and flatness control system. United Engineering, Inc., Pittsburgh, USA
4. Shan XY, Liu HM, Jia CY, Sun JL (2012) Flatness and profile integration control model for tandem cold mills. J Iron Steel Res Int 19(3):31-37
5. Yang GH, Cao JG, Zhang J, Song P, Yan TL, Rao KF (2012) Profile and flatness control technology with a long shifting stroke on wide non-oriented electrical steel sheets. J Iron Steel Res Int 19(1):31-35
6. Stone MD (1965) Theory and practical aspects in crown control. Iron Steel Engineer 8:73-90
7. Shohet KN, Townsend NA (1968) Roll bending methods of crown control in four high plate mills. J Iron Steel Inst 1088-1098
8. Jiang ZY, Zhu HT, Tieu AK (2005) Study of work roll edge contact in asymmetrical rolling by modifid influence function method. J Mater Process Technol 162-163:512-518
9. He A, Zhang Q, Xu J (2004) Shape control performance of 1800 virtual mills. J Univ Sci Technol Beijing 26:91-94
10. Ginzburg VB (1994) Profile and flatness of flat rolled products - part I. United Engineering, Inc., Pittsburgh, USA
11. Mori K, Osakada K, Oda T (1982) Simulation of plane-strain rolling by the rigid-plastic finite element method. Int J Mech Sci 24:519-527
12. Chandra S, Dixit US (2004) A rigid-plastic finite element analysis of temper rolling process. J Mater Process Technol 152:9-16
13. Zhang Q, Sun X, Bai J (2007) Analysis of rolls' elastic deformation on 6-h CVC mill by FEM. China Mech Eng 18:789-791
14. Salganik V (2002) Mathematical modeling of roll load and deformation in a four-high strip mill. J Mater Process Technol 125:695-699
15. Thole CA, Stüben K (1999) Industrial simulation on parallel computers. Parallel Comput 25:2015-2037
16. Liu X, Shi X, Li S, Xu J, Wang G (2007) FEM analysis of rolling pressure along strip width in cold rolling process. J Iron Steel Res Int 14(5):22-26

17. Wang X, Li F, Li B, Dong L, Zhang B (2012) Design and application of an optimum backup roll contour configured with CVC work roll in hot strip mill. ISIJ Int 52:637-1643
18. Ginzburg VB, Ballas R (2000) Flat roll fundamentals. Marcel Dekker, Inc., New York, USA
19. Lu C, Tieu AK, Jiang Z (2002) A design of a third-order CVC roll profile. J Mater Process Technol 125-126:645-648
20. Jiang Z, Wang G, Zhang Q (1993) Shifting roll profile and control characteristics. J Mater Process Technol 37:53-60
21. Kobayashi S, Oh SI, Altan T (1989) Metal forming and finite element method. Oxford University Press, New York, USA
22. Yanagimoto J, Kiuchi M (1998) General purpose FEM simulator for the three-dimensional deformation analysis of strip, bar/wire and shape rolling processes. In: Proceedings of the 7th International Conference on Steel Rolling (STEEL ROLLING' 98), Chiba, Japan
23. Jiang ZY, Zhu HT, Tieu AK, Sun WH (2004) Modeling of work roll edge contact in thin strip rolling. J Mater Process Technol 155-156:1280-1285
24. Jiang ZY, Tieu AK (2001) A simulation of three-dimensional metal rolling processes by rigid-plastic finite element method. J Mater Process Technol 112:144-151
25. Zienkiewicz OC, Taylor RL (2000) The finite element method, fifth edition, volume 1: the basis. Butterworth-Heinemann, Oxford, UK
26. Du XZ (2009) Research on mechanics of edge drop and its control technology in cold strip mill for high precision silicon steel. University of Science and Technology Beijing, China
27. Hu P, Ma N, Liu LZ, Zhu YG (2013) Theories, methods and numerical technology of sheet metal cold and hot forming: analysis, simulation and engineering application. Springer, London, UK
28. Gu TQ, Tang CL, Wang KJ (2010) The research of integrated control of flatness and transversal thickness deviation of the cold rolled strip. In: Proceedings of the 10th International Conference on Steel Rolling, Metallurgical Industry Press, Beijing, China
29. Shoji K, Miura H, Takeda E (1987) Profile and shape control in hot strip mill. In: Proceeding of the 4th International Steel Rolling Conference, Deauville, France
30. Ginzburg VB, Azzam M (1996) Selection of optimum strip profile and flatness technology for rolling mills. Iron Steel Engineer 19:30-35

Figure Captions:

Fig. 1 Schematic diagram for CVC 6 high cold rolling mill

Fig. 2 Radius variation with the width of rolls, (a) WR, (b) IMR, and (c) BR

Fig. 3 Unit volume stress state

Fig. 4 Schematic diagram for FEM model of CVC 6-high cold rolling mill

Fig. 5 Deformation resistance curve of strip

Fig. 6 Stress contour of 6-high CVC rold rolling mill

Fig. 7 Rolling force distribution between (a) BR and IMR, (b) IMR and WR, and (c) WR and strip of the third pass at the bottom side

Fig. 8 Measured positions of the inter-stand samples: (a) overview of the sample, and (b) measure across the whole width of exit side from OS to DS

Fig. 9 Variations of strip profile with the width of strip: (a) incoming material, (b) after pass1, (c) after pass2, (d) after pass 3, (e) after pass 4, and (f) after pass 5

Fig. 10 Schematic diagram of strip cross-section

Fig. 11 Crown control ability by WR bending force

Fig. 12 Crown control ability by IMR bending force

Fig. 13 Crown control ability by IMR shifting value

Fig. 14 Edge drop control ability by WR bending force

Fig. 15 Edge drop control ability by IMR bending force

Fig. 16 Edge drop control ability by IMR shifting value

Fig. 17 Distributions of rolling force and strip profile regarding IMR shifting value: (a)pressure between IMR and WR, (b)pressure between WR and strip, (c)strip profile across the width of strip, and (d)strip crown and strip edge drop

Table Captions:

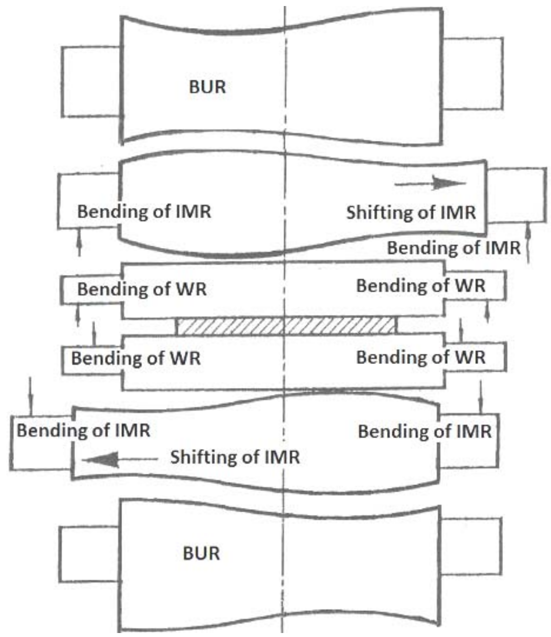

Fig. 1 Schematic diagram for CVC 6 high cold rolling mill

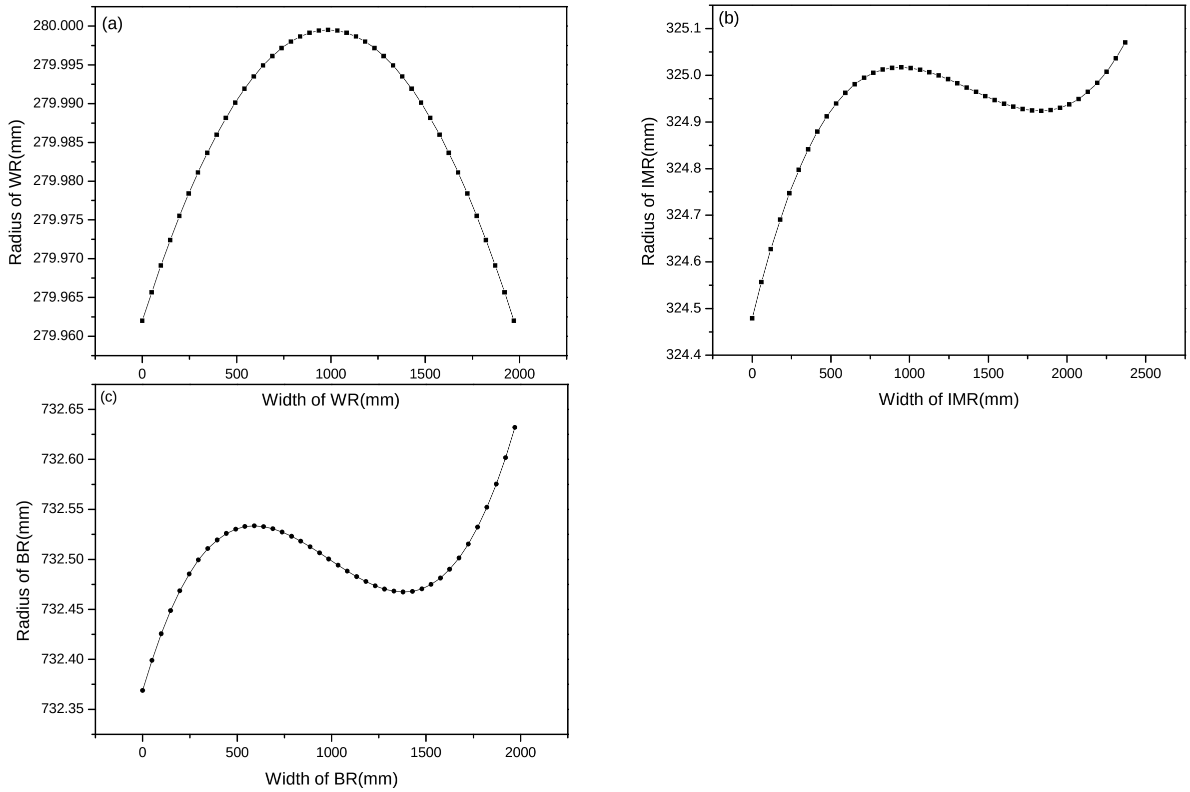

Fig. 2 Radius variation with the width of rolls. (a) WR, (b) IMR, and (c) BR

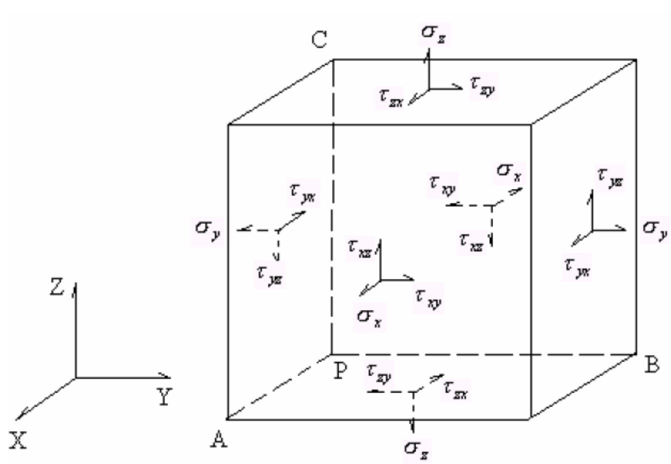

Fig. 3. Unit volume stress state.

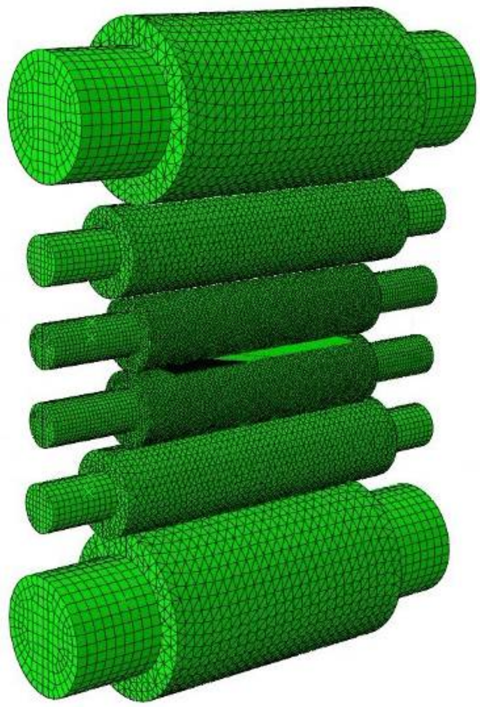

Fig. 4 Schematic diagram for FEM model of CVC 6-high cold rolling mill

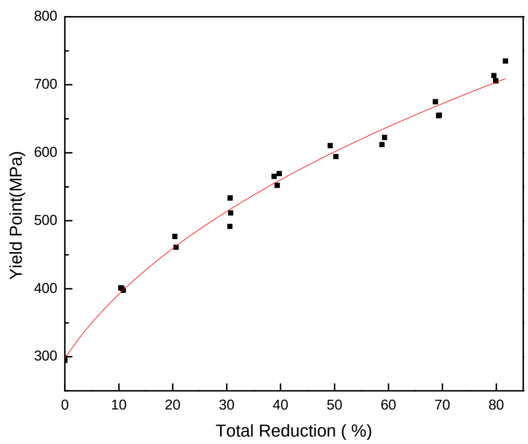

Fig. 5 Deformation resistance curve of strip

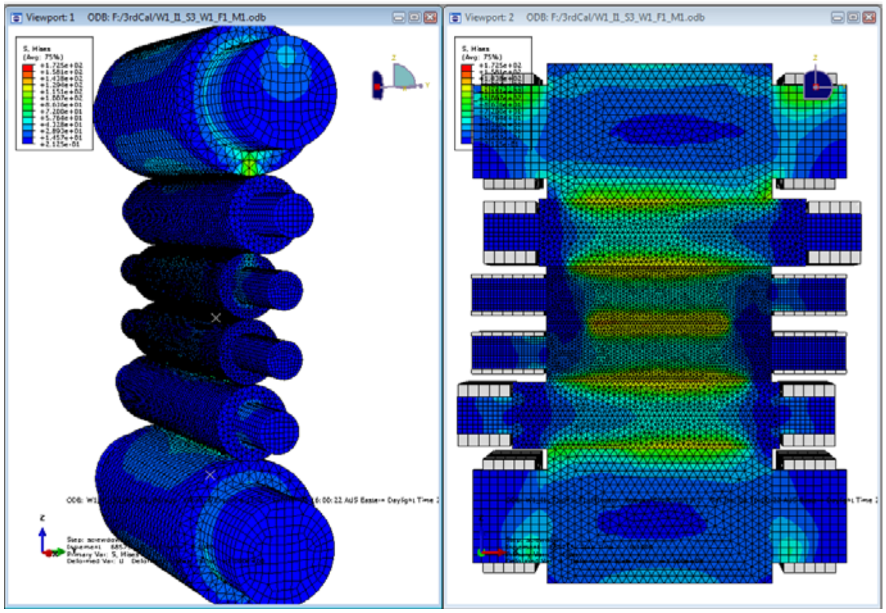

Fig. 6 Stress contour of 6-high CVC rold rolling mill

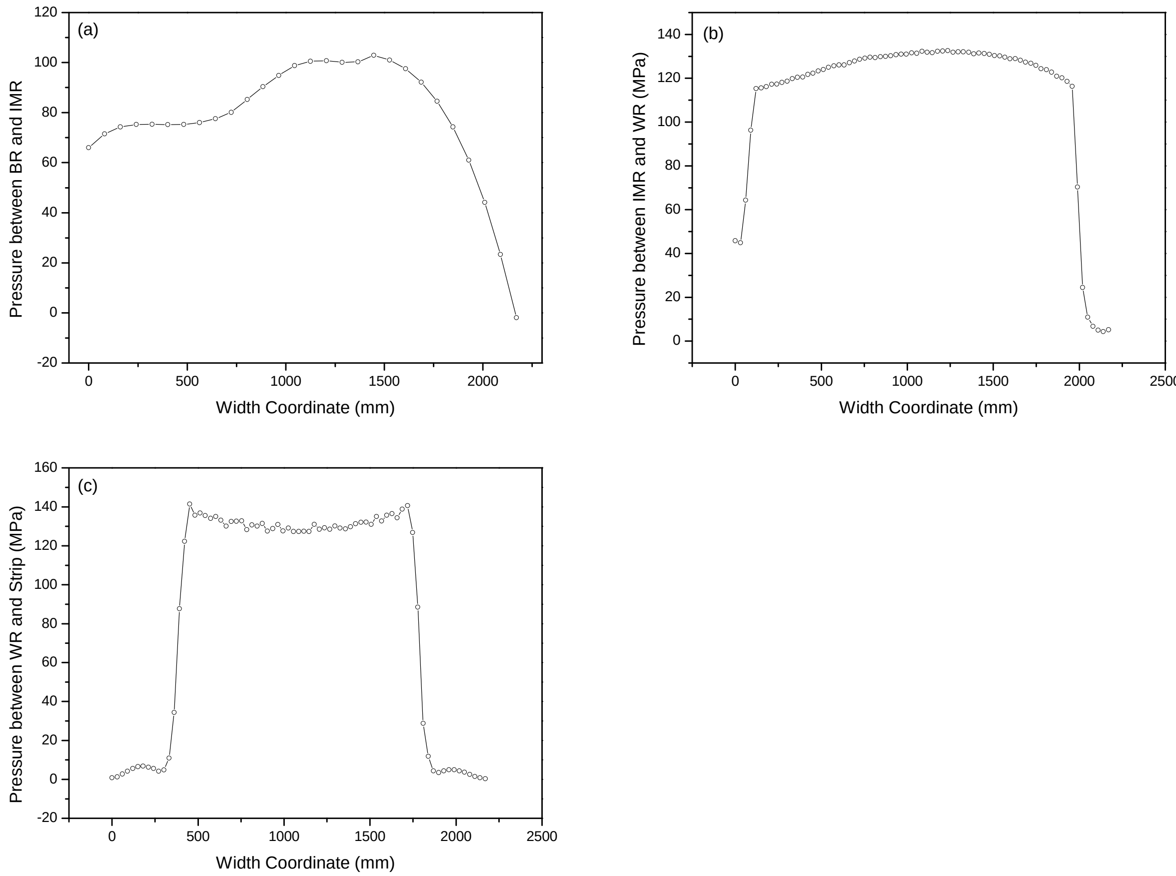

Fig. 7 Rolling force distribution between (a) BR and IMR, (b) IMR and WR, and (c) WR and strip of the third pass at the bottom side

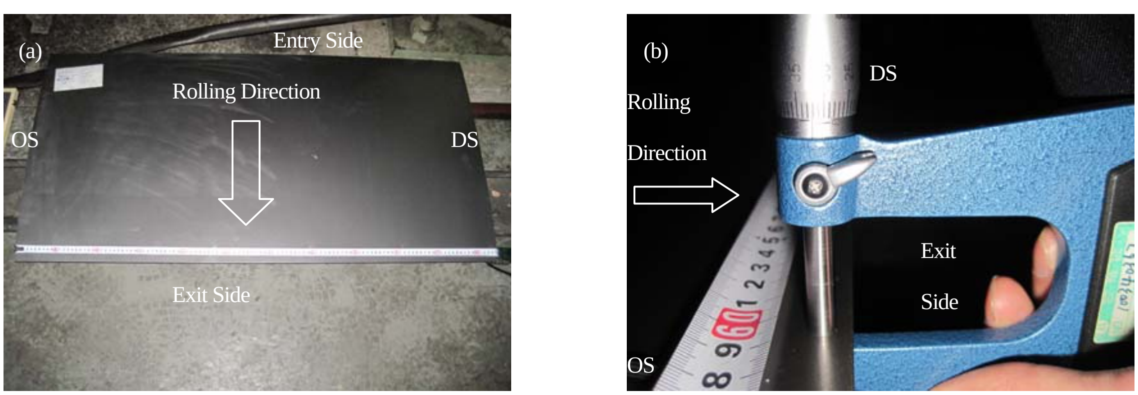

Fig. 8 Measured positions of the inter-stand samples: (a) overview of the sample, and (b) measure across the whole width of exit side from OS to DS

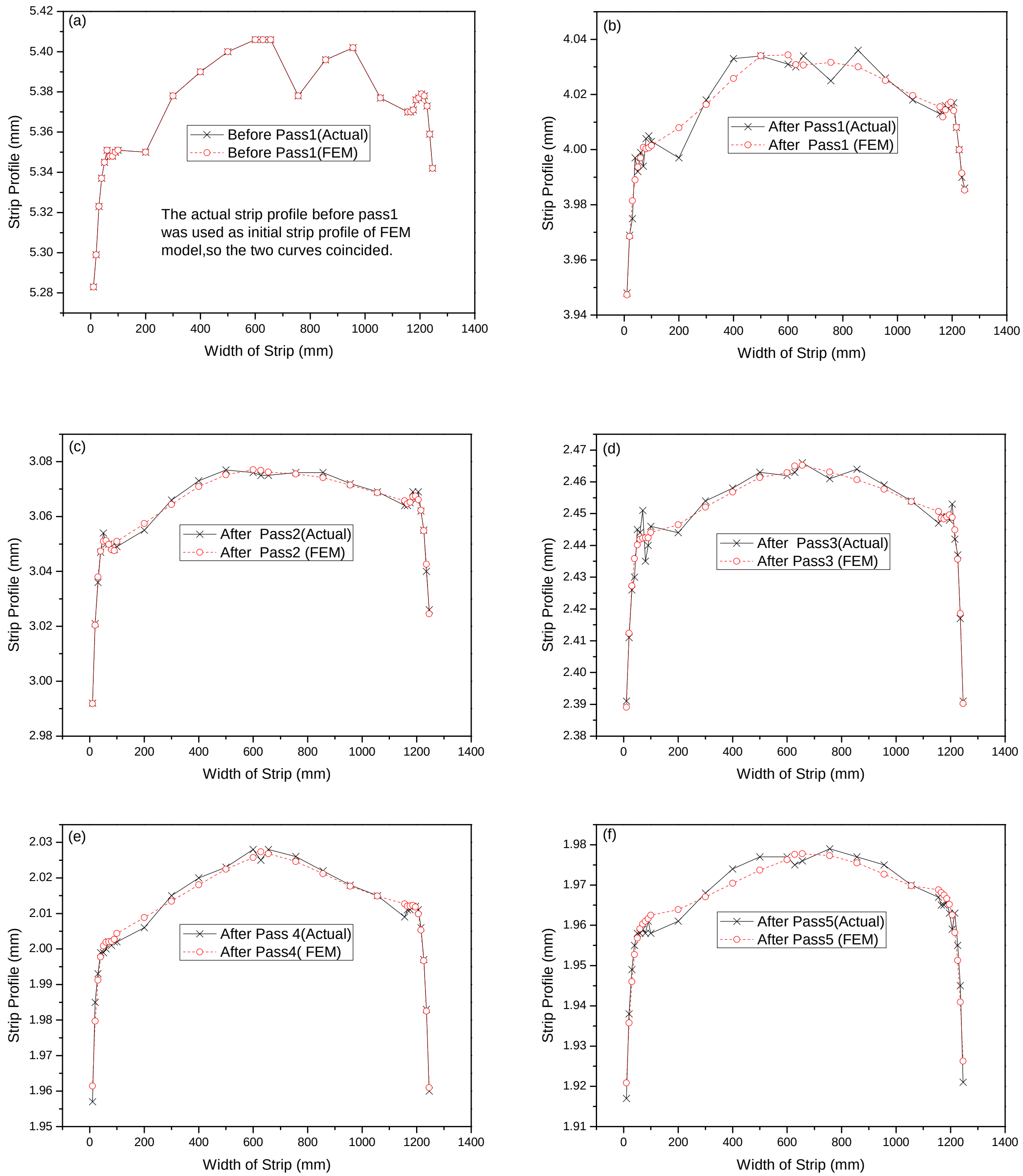

Fig. 9 Variations of strip profile with the width of strip: (a) incoming material, (b) after pass 1, (c) after pass 2, (d) after pass 3, (e) after pass 4, and (f) after pass 5

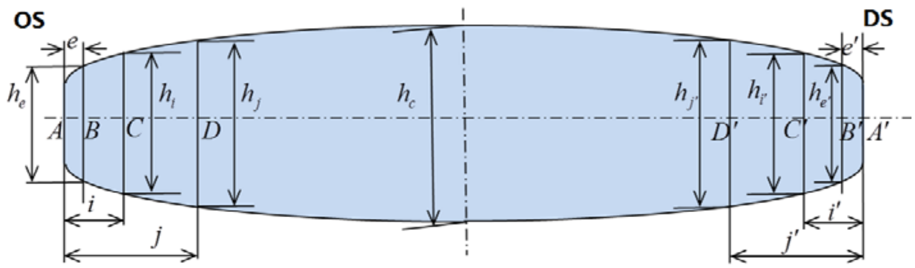

Fig. 10 Schematic diagram of strip cross-section

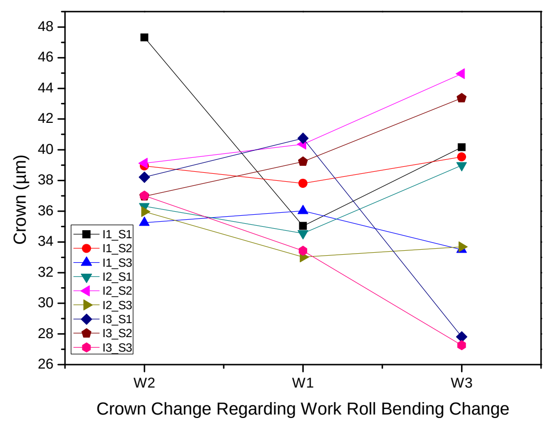

Fig. 11 Crown control ability by WR bending force

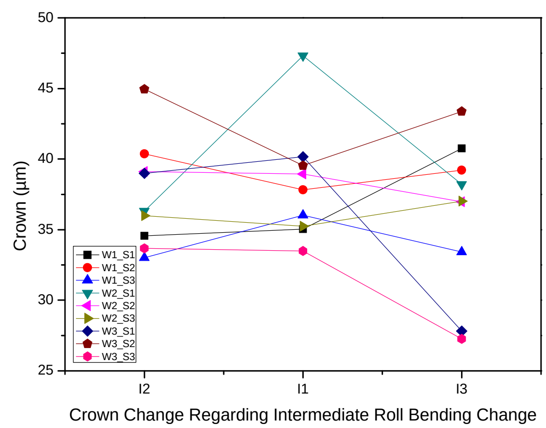

Fig. 12 Crown control ability by IMR bending force

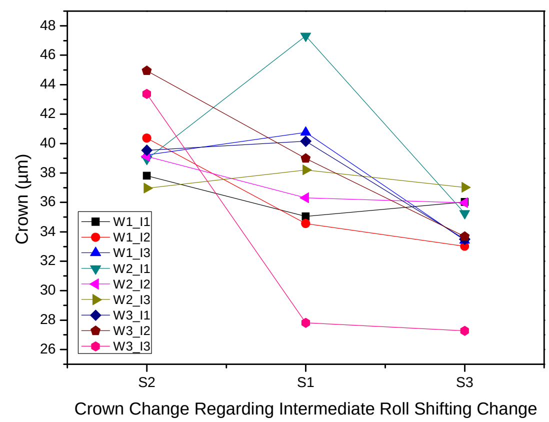

Fig. 13 Crown control ability by IMR shifting value

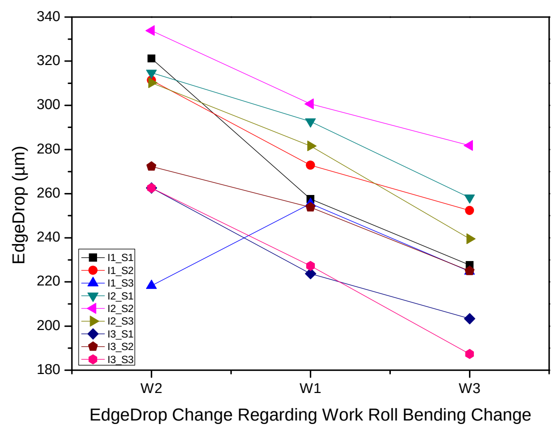

Fig. 14 Edge drop control ability by WR bending force

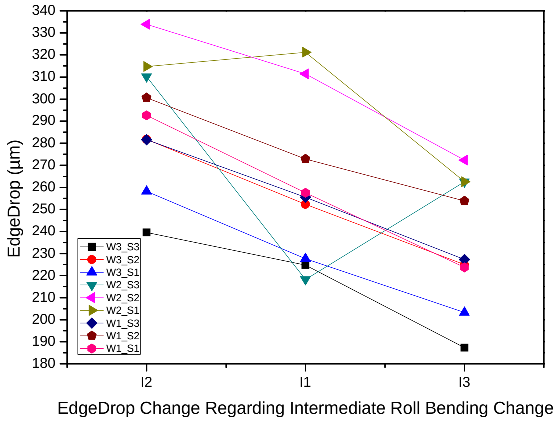

Fig. 15 Edge drop control ability by IMR bending force

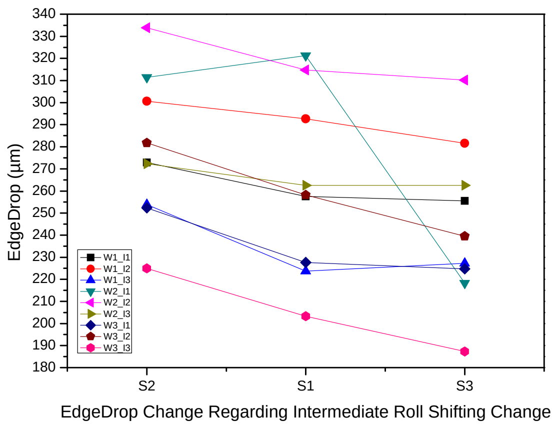

Fig. 16 Edge drop control ability by IMR shifting value

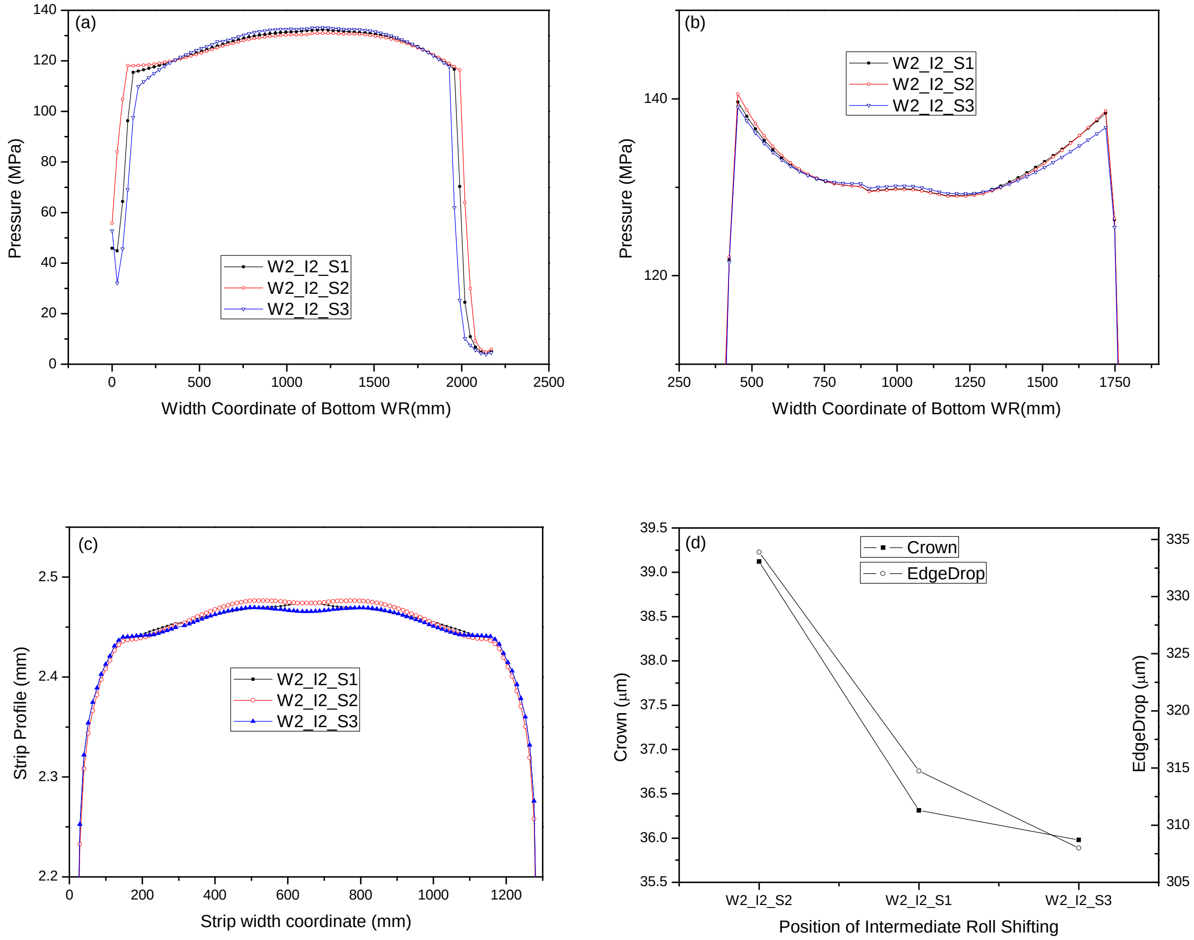

Fig. 17 Distributions of rolling force and strip profile regarding IMR shifting value: (a) pressure between IMR and WR, (b) pressure between WR and strip, (c)strip profile across the width of strip, and (d)strip crown and strip edge drop

Table 1 Parameters of roll set of 6-high CVC cold rolling mill

Items	Length of roll	Diameter（mm）	Hardness (HRC)	Curve
WR	1970	560-480	89-93.5	Parabolic
IMR	2370	650-570	77-80	CVC plus
BR	1970	1465-1300	66-70	CVC

Table 2 Mechanical properties of rolls for the FEM model

Roll type	E	μ	ρ	Material
WR	210 GPa	0.3	7 860 Kg/m^3	Alloy forged steel
IMR	210 GPa	0.3	7 860 Kg/m3	Alloy forged steel
BR	210 GPa	0.3	7 860 Kg/m3	Alloy forged steel

Table 3 Experimental data of the deformation resistance

Reduction/%	σ_s /MPa	Reduction/%	σ_s /MPa	Reduction/%	σ_s /MPa	Reduction/%	σ_s /MPa	Reduction/%	σ_s /MPa
0	297.958	20.4	476.964	39.4	552.022	59.3	622.548	79.9	705.827
10.4	401.460	30.6	491.586	49.2	610.607	69.3	654.520	81.7	734.745

Table 4 Coefficients of deformation resistance model

a_1	a_2	a_3
124.21327	9.65792	0.38578

Table 5 5-pass rolling schedule of 6-high CVC rolling mill

No. of pass	Entry Thickness (mm)	Exit Thickness (mm)	Bending of WR (KN)	Bending of IMR (KN)	Shifting of IMR (mm)	Entry Tension (KN)	Exit Tension (KN)	Reduction Of Pass (%)
1	5.400	4.085	696.1	1267.8	-112.8	242.6	546.5	24.344
2	4.085	3.111	641.6	1169.9	-134.1	546.5	475.7	23.832
3	3.111	2.458	547.8	1171.8	-137.3	475.7	422.7	21.013
4	2.458	2.048	401.2	1159.5	118.75	422.7	404.5	16.657
5	2.048	1.966	2.8	78.2	-142.5	404.5	107.0	2.368

Table 6 Definition of the flatness control symbol

Symbol	Flatness actuator	Values of n in symbol	Remark
W_n	Bending force of WR	2，1，3	2：Min(-700KN)；1：0；3：Max(1000KN)
I_n	Bending force of IMR	2，1，3	2：Min(-900KN)；1：0；3：Max(1300KN)
S_n	Shifting value of IMR	2，1，3	2：Min (-160mm)；1：0 mm；3：Max(160mm)

Note: n represents the different value of actuators. "2" stands for minimum, "1" stands for zero, and "3" stands for maximum.

Table 7 Non-uniform coefficient for different shifting value

non-uniform coefficients	$W_2\_I_2\_S_2$	$W_2\_I_2\_S_1$	$W_2\_I_2\_S_3$
β_{iw}	1.137013891	1.175604537	1.207581627
β_{ws}	1.630818895	1.625476427	1.614986388
β_{sp}	1.021637	1.019481616	1.00997896